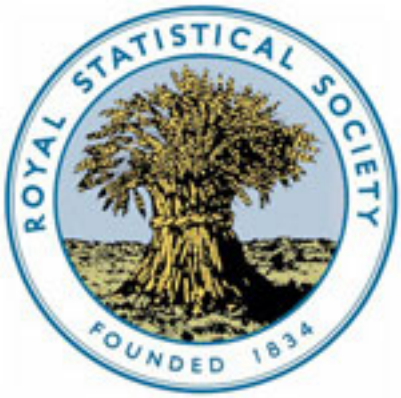

Appl. Statist. (1983),
32, *No.* **1**, *pp.* 51–63

The Interpretation of Process from Pattern using Two-dimensional Spectral Analysis: Methods and Problems of Interpretation

By E. RENSHAW† and E. D. FORD

University of Edinburgh, UK *Institute of Terrestrial Ecology, UK*

[Received February 1982. Final revision December 1982]

SUMMARY

Two-dimensional spectral analysis provides a comprehensive description of both the structure and scales of pattern in a spatial data set. It assumes no structural characteristics in the data prior to analysis. We demonstrate the advantage of this in an ecological situation where pattern may exist over a range of scales, be anisotropic and non-stationary. All these may be important features relating to the underlying biological and environmental pattern generating mechanisms and should be explained prior to model building. We discuss general problems of estimation, discrimination and interpretation of spectra and illustrate them through the analysis of a forest canopy data set.

Keywords: SPATIAL ANALYSIS; SCALES OF PATTERN; TWO-DIMENSIONAL CARTESIAN AND POLAR SPECTRA; POINT AND LATTICE SPECTRA; AUTOCORRELATIONS; ANISOTROPY; NON-STATIONARITY; ECOLOGY; FOREST CANOPIES

1. INTRODUCTION

Spectral analysis in two dimensions has found extensive application in the processing of electronic signals, largely in connection with the design of filters with specific frequency response characteristics (Rabiner and Gold, 1975). Other applications include: the reconstruction of transmitted photographic data from weather satellites and air reconnaissance photographs; the analysis of medical X-rays and electron micrographs; and the description of magnetic, oceanographic and gravitational data. Optical techniques (Lugt, 1974) provide an alternative to using a digital computer.

These applications are concerned with the generation and manipulation of spectra of complex patterns from the natural environment, but rarely with *interpretation* of the *information* they contain *in relation to processes generating pattern*. The spectra are seldom used to infer models of the processes which cause pattern, and only a few such attempts have been made. For example, Bartlett (1964, 1975) calculated the two-dimensional point spectra of two stands of Japanese black pine saplings and inferred an inhibition process between plants. McBratney and Webster (1981) analysed the yields of wheat grain and straw obtained by Mercer and Hall (1911), and showed periodic effects attributed to an earlier ridge and furrow system.

Wider application of this potentially useful *interrogative* technique has been impeded by three problems: (i) large data sets, frequently gathered in spatial analysis, can require extensive computational effort; (ii) assessment of apparent spectral structure; and, (iii) subsequent interpretation. Our purpose is to present an account of how two-dimensional spectral analysis may

†*Present address*: Department of Statistics, University of Edinburgh, King's Buildings, Mayfield Road, Edinburgh EH9 3JZ.

 0035–9254/83/32051 $2.00

be applied, and to provide some solutions to these three problems through the analysis of a data set of forest canopy heights. Analyses of other ecologically based data sets will appear subsequently.

2. CALCULATION OF THE EMPIRICAL AUTOCOVARIANCE AND SPECTRAL FUNCTIONS

2.1. *Autocovariance and Spectral Functions*

Let X_{st} $(s = 1, \ldots, m; t = 1, \ldots, n)$ denote a two-dimensional array of observations corrected for their overall mean. We define the sample autocovariance at lag (j, k) by

$$C_{jk} = (1/mn) \sum_{s=1}^{m-j} \sum_{\Omega_t} X_{st} X_{s+j,\, t+k}, \tag{2.1}$$

where $\Omega_t = \{1, \ldots, n-k; k \geqslant 0\}$ and $\Omega_t = \{-k+1, \ldots, n; k < 0\}$. For $j, k \geqslant 0$ it is easily verified that $C_{-j,-k} = C_{j,k}$ and $C_{-j,k} = C_{j,-k}$, so we need only consider $j = 0, \ldots, m-1$. For a general account of spatial autocovariance see Cliff and Ord (1981).

Autocovariances are themselves dependent and this can lead to problems of interpretation. However, to a large extent difficulties due to such dependences may be overcome by calculating the Fourier transform of (2.1), namely

$$f(\omega_1, \omega_2) = \sum_{j=-m+1}^{m-1} \sum_{k=-n+1}^{n-1} C_{jk} \cos(j\omega_1 + k\omega_2). \tag{2.2}$$

This function, called the sample spectral function or periodogram, is usually evaluated at the Fourier frequencies $(\omega_1, \omega_2) = (2\pi p/m, 2\pi q/n)$ where $p = 0, \ldots, m-1$; $q = 0, \ldots, n-1$. For large data matrices, of the order 100×100 for some machines, direct use of (2.2) will give rise both to unacceptable computing time and round-off error.

By taking the Fourier transform of the mean-corrected data matrix a form of $f(\omega_1, \omega_2)$ can be derived which is far quicker to evaluate than (2.2) and is less subject to round-off error. Define

$$I_{pq} = mn(a_{pq}^2 + b_{pq}^2), \tag{2.3}$$

where p and q are integers and

$$a_{pq} + ib_{pq} = (1/mn) \sum_{s=1}^{m} \sum_{t=1}^{n} X_{st} \exp\{2\pi i \left(\frac{ps}{m} + \frac{qt}{n}\right)\}. \tag{2.4}$$

Then a little algebra shows that

$$I_{pq} \equiv f(2\pi p/m, 2\pi q/n) \tag{2.5}$$

and so (2.3) provides an alternative method of computing the sample spectrum. The basic theory of two-dimensional spectral analysis (see Ripley, 1981) is a straightforward generalization from one-dimension, details of which may be found, for example, in Jenkins and Watts (1968).

As $I_{m-p,\,q} = I_{p,\,n-q}$ then a suitable form in which to output the periodogram $\{I_{pq}\}$ is a matrix array with $p = 0, \ldots, m/2$ and $q = -n/2, \ldots, n/2 - 1$. The cosine waves

$$X_{st} = \cos\left[2\pi \left(\frac{ps}{m} \pm \frac{qt}{n}\right)\right]$$

give rise to single spikes in the periodogram at points $(p, \pm q)$, so the sign of q relates to the direction of travel (ϕ) of the waves. Here

$$\phi = \tan^{-1}(np/mq) \quad (0 \leqslant \phi < \pi) \tag{2.6}$$

and the associated wavelength is $mn/\sqrt{(m^2q^2 + n^2p^2)}$. Moreover,

$$\sum_{p=0}^{m-1}\sum_{q=0}^{n-1} I_{pq} = \sum_{s=1}^{m}\sum_{t=1}^{n} X_{st}^2 = \sigma^2 mn, \tag{2.7}$$

and so I_{pq}/mn is the variance attributable to the component with frequency $(2\pi p/m, 2\pi q/n)$.

Choice of m and n requires a careful balance between computational convenience, man-hours available for data collection and problems posed due to aliasing. The highest resolvable row (p) and column (q) values (the Nyquist frequencies) are $m/2$ and $n/2$; variability which belongs to higher, unresolvable frequencies is forced into lower frequencies thus confounding them. Consequently sampling must be sufficiently intense to detect the smallest scale of pattern, and the total area sampled large enough to include all patterns of interest.

Unless the data size mn is excessively large computation of (2.3) is not unduly expensive. If necessary, however, for m and n powers of 2 $\{I_{pq}\}$ may be evaluated far more quickly by means of the Fast Fourier Transform (FFT). There are several one-dimensional FFT programs available, for example FASTF (Monro, 1975), and two-dimensional Fourier coefficients may be obtained by means of the subroutine FT2D (Monro, 1971). If the data are collected with spectral analysis in mind, then it may be possible to ensure that m and n are powers of 2, but if not then the Chirp-transform (Monro and Branch, 1977) – in conjunction with, for example, CFOR2 (Branch, 1973) – allows general lengths m and n. The time penalty by comparison with the FFT is not severe, and is far less than that imposed by (2.2). To aid interpretation of large periodograms we may either: (i) form totals of the $\{I_{pq}\}$ in contiguous blocks, this corresponds to simple uniform smoothing; or (ii) use local polynomial smoothing to estimate spectral values on a conveniently coarse grid of frequencies.

The FFT may also be used to evaluate the autocorrelation function (2.1). First, embed the $m \times n$ matrix $\{X_{st}\}$ in the first quadrant of a $2m \times 2n$ matrix of zeros and evaluate $\{I_{pq}\}$ for $p = 0, \ldots, 2m-1$; $q = 0, \ldots, 2n-1$. Second, calculate the inverse FFT

$$L_{jk} = \sum_{p=0}^{2m-1}\sum_{q=0}^{2n-1} I_{pq} \exp\{-\pi i\left(\frac{pj}{m} + \frac{qk}{n}\right)\}$$

by using, for example, FASTF and FT2D with m and n replaced by $-2m$ and $-2n$, respectively. Then $C_{j,k} = (1/mn)L_{j,k}$ for $0 \leqslant j < m$; $0 \leqslant k < n$, and $C_{j,-k} = (1/mn)L_{j,2n-k}$ for $0 \leqslant j < m$; $0 < k < n$.

2.2. *Interpretation of the Spectrum*

A single spike in the spectrum at position (p, q) corresponds to a pure cosine wave. In general more than one feature will be present in the spectrum, and Ford (1976) presents examples of simple spatial patterns which give rise to several isolated peaks. Further examples may be computed at will. Hence given a particular spectrum, comparison with known forms is an obvious first step towards an interpretation.

To illustrate the power of spectral analysis consider a process developing under a directional stimulus, for example

$$X_{st} = \sum_{p=0}^{m/2}\sum_{q=-n/2}^{n/2-1} g_{pq} \cos\left[2\pi\left(\frac{ps}{m} + \frac{qt}{n}\right) + \psi_{pq}\right],$$

where $\{g_{pq}\}$ decays away from the line $q = k + p \tan\theta$ and $\{\psi_{pq}\}$ are i.i.d. $U[0, 2\pi)$ random variables. Fig. 1a shows the result of a simulation run with $g_{pq} = \exp\{-|q - k - p\tan\theta|\}$ for $\theta = 20^\circ$ and $k = -6$, and in spite of the visually complex structure of the $\{X_{st}\}$ the periodogram (Fig. 1b) shows a very clear ridge running from $I_{0,-6} = 5.75$ per cent (of total variance) to

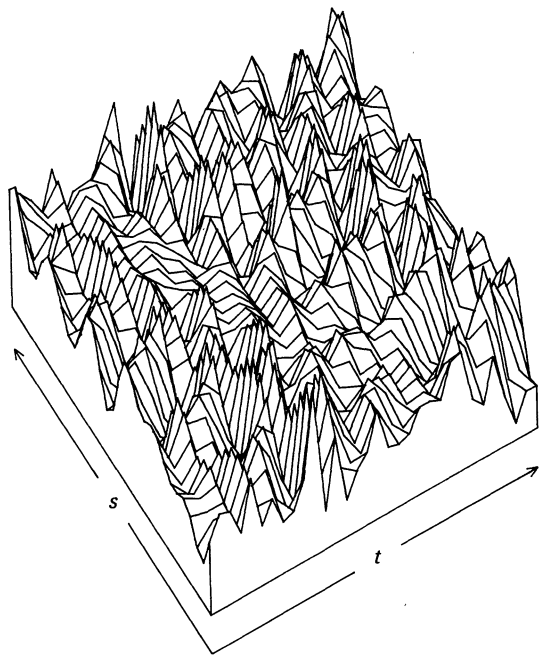

(a)

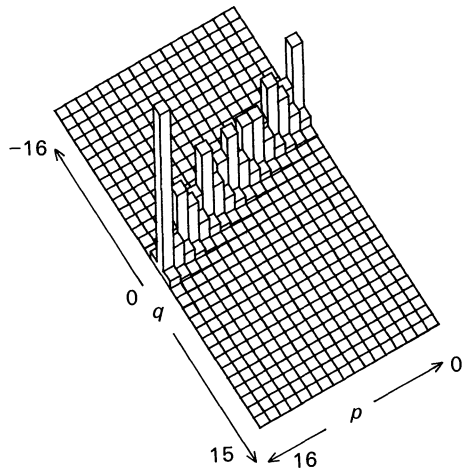

(b)

Fig. 1. Simulation of a process with a strong directional component (see text.)
(a) Generated values, (b) the associated spectrum.

$I_{16,0} = 6.37$ per cent. The maximum value of I_{0q} is at $q = -6$, as expected, and the angle θ to the $q = 0$ axis is $\tan^{-1}(6/16) = 20^\circ\ 33'$ virtually identical to the value used. Note that whilst the overall ridge-feature is strikingly apparent the individual ridge values show considerable variation.

2.3. *Transformation of the Periodogram into Polar Components*

Data from the natural environment often possesses a directional component which may be apparent from the Cartesian spectrum. Transformation of the Cartesian spectrum $\{I_{pq}\}$ $(p = 0, \ldots, m/2; q = -n/2, \ldots, n/2 - 1)$ into a polar system enables directional components and scales of pattern to be represented separately. First denote $G_{r\theta} \equiv I_{pq}$ where $r = \sqrt{(p^2 + q^2)}$ and $\theta = \tan^{-1}(p/q)$, and then combine these $G_{r\theta}$ values into polar segments. We have found the subdivision $-5^\circ < \theta \leqslant 5^\circ, 5^\circ < \theta \leqslant 15^\circ, \ldots, 165^\circ < \theta \leqslant 175^\circ$ together with $0 < r \leqslant 1, 1 < r \leqslant 2, \ldots$ appropriate. As different segments contain different numbers of entries the resulting polar-spectrum should be scaled by the number of elements in each segment, which also provides some degree of smoothing. These counts are easily obtained from the polar representation of the $m \times n$ matrix $I'_{pq} \equiv 1$ with $I'_{00} = 0$. We see from (2.7) that on dividing the full periodogram $\{I_{pq}\}$ by $\sigma^2 mn/(mn - 1)$ each element (except I_{00}) has expected value unity under the null hypothesis of spatial randomness, and so therefore has each of the scaled polar segments. However the precision for each segment will vary with the number of elements it contains. As row and column Nyquist frequencies are $m/2$ and $n/2$, respectively, care is required when interpreting r values with $r > \min(m/2, n/2)$. The unrestricted Nyquist frequency is $(m/2, n/2)$ with $r = (1/2)\sqrt{(m^2 + n^2)}$ and wavelength $\sqrt{2}$.

2.4. *Point Spectra*

Where the spatial locations of data points have been recorded as two-dimensional co-ordinates we may approximate positions to the nearest point of a fine lattice laid on the study area and use the techniques described earlier. An alternative exact technique has been introduced by Bartlett (1964, 1978). Denote $N(\mathbf{r})$ to be the cumulative number of points at position $\mathbf{r}$ with $E\{dN(\mathbf{r})\} = \lambda \mathbf{dr}$, where $dN(\mathbf{r})$ is either 0 or 1. Then we evaluate the periodogram $I_{pq} = J_{pq} J^*_{pq}$ where * denotes complex conjugate and

$$J_{pq} = \sqrt{(2/n)} \sum_{s=1}^{n} \exp\{(2\pi i/n)(px_s + qy_s)\}, \tag{2.8}$$

the sample having co-ordinates $\mathbf{r}_s \equiv (x_s, y_s)$ $(s = 1, \ldots, n)$. If the spectrum is assumed to be isotropic, with $\omega = |\boldsymbol{\omega}|$, then the I_{pq} may be averaged to give

$$I'(\omega) = 2 + (2/n) \sum_{r \neq s} J_0(\omega d_{rs}), \tag{2.9}$$

where $J_0(x)$ is a standard Bessel function and $d_{rs} = \sqrt{\{(x_s - x_r)^2 + (y_s - y_r)^2\}}$. Unfortunately this does not reduce the calculations. Use of $I'(\omega)$ also introduces bias, the expected value of $I' - 2$ is approximately $16/(n^2 \omega^3)$.

3. SCOTS PINE FOREST

As a forest grows the branching structure, and therefore the shape of individual tree crowns, is affected by direct environmental influences (e.g. Cochrane and Ford, 1978) which may be modified by the presence of neighbours either through mutual shelter or competition effects (e.g. Ford and Deans, 1978). The canopy structure of a 39-year thinned commercial plantation of Scots pine (*Pinus sylvestris* L.) at Thetford Forest, UK containing 1000 trees · ha^{-1} was investigated. An area 36 m × 120 m was surveyed. Horizontal extent of the individual tree crowns was measured along parallel transects spaced at 1 m intervals. Height and location of each tree, and

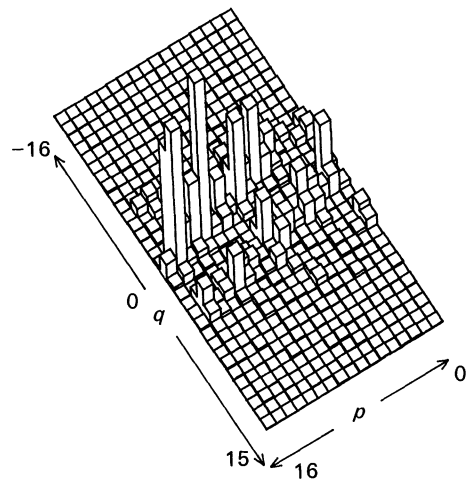

Fig. 2. The spectrum of a 32 × 32 sub-matrix from the Thetford canopy height data.

crown height at its perimeter, were measured; crown height at intermediate distances between perimeter and trunk was estimated by geometric projection (Ford, 1976).

3.1. *Assessment of Spectral Features*

We restrict our initial attention to a 32 × 32 sub-matrix of canopy heights. The resulting spectrum was calculated (Section 2.1), and the relative values of $\{I_{pq}\}$ are shown in Fig. 2. There is visual evidence of two parallel ridges, and to determine their extent let us place $I_{pq} = 0$ for all values (p, q) for which I_{pq}, when expressed as a percentage of total variance, is less than some value c. With $c = 1.0$ per cent only 56 per cent of total variation is explained, and just the tops of the two spectral ridges show. As c is decreased more of the ridge-structure becomes apparent, with no apparent new detail being shown when $c < 0.4$ per cent. A value of 0.4 per cent enables just 10 per cent of the spectral values to explain 73 per cent of the total variance, and we retain it as the "critical-value".

We stress that we are presenting two-dimensional spectral analysis as an *exploratory* technique which can be used to interrogate a spatial data set for pattern. It is particularly appropriate at that stage of an investigation when hypotheses are being generated about the mechanisms which underlie the development of a spatial pattern. In this particular context we are therefore concerned far more with the construction and "biological significance" of these two spectral ridges than with their "statistical significance"; a more sophisticated statistical analysis of the ridges could be made via the $P(\lambda, \mu)$ test of Priestley (1964).

3.2. *Features in the Canopy Height Spectrum*

Two main features are apparent (Fig. 2), which together contribute 71.6 per cent of the total variance.

I. A ridge in the positive quadrant which has two parts. A low frequency ridge (Ia) from (1, 0) to (8, 4) contributes 19.07 per cent, and the two large elements at (4, 1) and (8, 2) both have ϕ values of 76° — from (2.6) $\phi = \tan^{-1}(p/q)$. Separated from Ia by a single row is a ridge of high frequency elements (Ib) which contributes 6.09 per cent, and the peak value is 1.78 per cent at (12, 4) with $\phi = 72°$.

II. A ridge in the negative quadrant from $(4,-4)$ to $(15, 1)$ ($\phi = 135°$ to $86°$) contributes 46.4 per cent. The high frequency elements are mainly clustered between $90°$ and $95°$, and so reflect a basic row effect. A plot of the number of zeros in each row of the data against row number (1 to 32) clearly showed the presence of two cyclic components: a low frequency cycle of wavelength 21 rows and a high frequency oscillation with 11 complete cycles occurring over 25 rows. This latter cycle corresponds to a wavelength of 2.3 m and a frequency of 14.1 which is near the centre of the group of high frequency components. The absence of canopy is clearly of major importance in its effect on spectral structure.

To relate the censoring value $c = 0.4$ per cent to more formal test procedures suppose the $\{X_{st}\}$ are i.i.d. $N(0, \sigma^2)$ random variables. Then it follows from (2.3) and (2.4) that $\{2I_{pq}/\sigma^2\}$ are distributed as χ^2_2. When the half-spectrum is expressed as a percentage of total variance, $\{\tilde{I}_{pq}\}$ say, then we require $E[\tilde{I}_{pq}] = 200/mn$ (per cent) whence $\{\tilde{I}_{pq}\}$ are distributed as $(100/mn)\,\chi^2_2$. Moreover, this result holds approximately true regardless of the distribution of the $\{X_{st}\}$. On a one-sided test we have:

Significance level (%)	*Critical value (%)*	*No. of elements in I*	*No. of elements in II*
–	(0.40)	(25)	(24)
10	0.45	23	21
5	0.59	18	15
1	0.90	13	14
0.1	1.35	5	10

where the critical values given are $(100/32^2) \times$ the upper percentage points of χ^2_2. The critical value $c = 0.4$ per cent for individual estimates is clearly unusually low by conventional criteria. This illustrates a major difference between one- and two-dimensional analyses. For whilst only a few spectral values in the former may constitute a "peak", many such values may be incorporated into a two-dimensional "spectral feature"; yet as periodogram estimates have high variance not all within a feature will necessarily be significant at say the 5 per cent or 1 per cent level. Our "censoring approach" avoids ill-defined features, yet excludes much background noise. Moreover, individual values may still be tested by χ^2_2 – 15 values exceed the 0.1 per cent significance level and range from 1.37 per cent to 7.44 per cent. Note that smoothing (Section 3.3) may be used as an additional aid to the identification of spectral features.

We have already seen from the simulated example (Figs 1a and 1b) that a directional stimulus may produce a spectral ridge. Ridge I contains the origin and represents families of cosine waves travelling at $\phi \simeq 72°$. To analyse ridge II we follow Priestley (1964) and first rotate the data set to enable this ridge to lie parallel to the axis $\omega_1 = 0$. For a rotation of the spectrum through an angle θ is equivalent to a rotation of $\{X_{st}\}$ through θ. Suppose the ridge now lies along the line $\omega_1 = \omega$, then the corresponding spectral density function may be written in the form $f(\omega_1, \omega_2) = \delta(\omega_1 - \omega)g(\omega_2)$ where $g(\omega_2)$ is a continuous function of ω_2 and $\delta(x)$ denotes the Dirac delta function. One model for the corresponding process $\{X_{st}\}$ is given by

$$X_{st} = H(t) \cos(2\pi\omega s/m + \psi_t), \tag{3.1}$$

where $H(t)$ is a stationary process with spectral density function $g(\omega_2)$.

Suppose that ridge II passes directly through the values 1.49 per cent at $(4,-4)$ and 6.51 per cent at $(15, 0)$, then $\phi = \tan^{-1}(11/4) = 70°$, virtually the same as for ridge I. The perpendicular distance from the origin to this ridge is $44/\sqrt{(13.7)} = 3.8$, so under an approximate rotation of $20°$ the line $\omega = \omega_1$ corresponds to $\omega \doteq 4$. Thus (3.1) becomes

$$X_{st} = H(t) \cos(\pi s/4 + \psi_t), \tag{3.2}$$

and the t-cosine waves are themselves modulated along their length, i.e. perpendicular to the direction of travel, by waves of constant wavelength (~ 8) but different phases (ψ_t).

Taken together ridges I and II strongly suggest the presence of a powerful directional component. They provide evidence for tree crowns being aligned in rows inclined at an angle of 70° to the direction of tree planting and these rows having a sinusoidal structure with wavelength approximately equal to 8 m. This structure was certainly not apparent when the canopy was viewed above from a meteorological mast.

The spectrum of the canopy presence/absence matrix closely resembles that for canopy heights. Both ridges appear in the same position as before, although their individual components are generally smaller, and the total percentage of explained variance has dropped from 73.4 to 64.4 per cent. The principal difference is the virtual disappearance of Ib and so this feature is most likely a consequence of the shape of the tree crowns themselves. For whereas the canopy height matrix will emphasize the shape of the tree crowns, the presence/absence matrix cannot. Separation of the foliage is a gradual process with increasing height but an important stage is recognized as the zero plane displacement of wind speed (Fig. 8, in Ford, 1976) which is estimated from meteorological measurements. At this height, 11.8 m, the mean crown diameter is 2.6 m, close to the mid point of the wavelength bandwidth of 2.1–3.1 m of feature Ib, and this further supports the interpretation of Ib as the Fourier representation of tree crown shape in the canopy.

3.3. *Smoothing the Spectrum*

Smoothing accentuates the visual effect of the two ridges (Fig. 2). First write (2.2) in the form

$$f(\omega_1, \omega_2) = \sum_{j=-P}^{P} \sum_{k=-Q}^{Q} w_{jk} C_{jk} \cos(j\omega_1 + k\omega_2) \tag{3.3}$$

for $P = m - 1$, $Q = n - 1$ and $w_{jk} \equiv 1$. A smoothed version of (3.3), $\hat{f}(\omega_1, \omega_2)$, may then be derived by a suitable choice of the truncation points $0 < P < m, 0 < Q < n$ and the weights $\{w_{jk}\}$. Huang (1972) has shown that good two-dimensional windows can be obtained from good one-dimensional windows, $\hat{w}$, via the relation $w_{jk} = \hat{w}\{\sqrt{(j^2 + k^2)}\}$. Thus they may be easily designed from known properties of one-dimensional windows (see, for example, Jenkins and Watts 1968): an excellent discussion of window functions, including the more sophisticated Kaiser window, is contained in Rabiner and Gold (1975). The optimum values P and Q represent a compromise, for they must be chosen subjectively to balance resolution against variance. If P and Q are too small, important features may be smoothed out, whilst if they are too large the behaviour of $\hat{f}(\omega_1, \omega_2)$ becomes erratic.

Smoothed spectra of the 32 x 32 Thetford canopy height data matrix were evaluated for $P = Q = 15$, 23 and 31 with various window functions, and Fig. 3 shows the result of using the one-dimensional Tukey window $w_{jk} = (1/2)[1 + \cos\{\pi[(j^2 + k^2)/2]^{1/2}/(P + 1)\}]$ with $P = Q = 15$. We found that with this choice of P and Q the separation of the spectrum into two distinct ridges was most clearly defined, though the relative importance of individual frequencies within the ridges is no longer apparent.

An alternative technique is to take any one-dimensional moving average row vector of weights $\mathbf{v}$ (quadratic or binomial coefficients, for example), form $\mathbf{v}^T\mathbf{v}$, and then smooth $\{I_{pq}\}$ directly. As the spectrum lies on a torus it is easily surrounded by the appropriate border to enable smoothing at the edges.

3.4. *The Autocorrelation Function of Canopy Heights*

The autocorrelation function $\{C_{jk}/\sigma^2\}$ of the 32 x 32 matrix of canopy heights (2.1 and Fig. 4) exhibits a strong cyclic row effect, with an approximately equal phase shift between successive rows, and has the appearance of two orthogonal systems of waves. The three largest autocorrelations are 1.00 at (0, 0); 0.54 at (2, 6) and 0.25 at (4, 13). Two cycles occur within

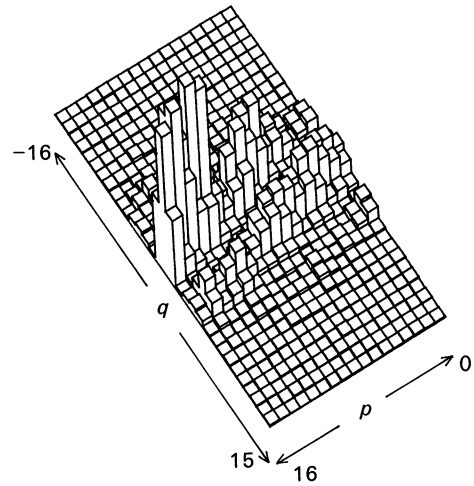

Fig. 3. Thetford spectrum smoothed by the one-dimensional Tukey window (see text.)

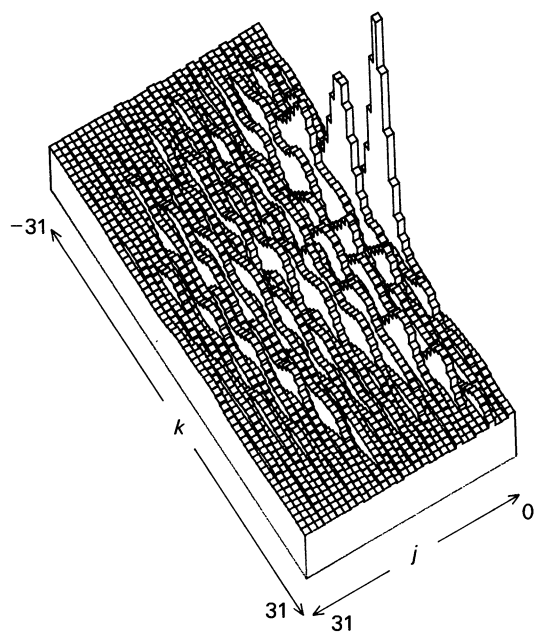

Fig. 4. The autocorrelation function $\{C_{jk}/\sigma^2\}$ for $0 \leqslant j \leqslant 31$, $-31 \leqslant k \leqslant 31$ calculated from the Thetford canopy height data.

$\sqrt{(4^2 + 13^2)} = 13.6$ m which corresponds to a wavelength of 6.8 m, close to the wavelength ($\sim$8 m) previously estimated for the perpendicular distance of the spectral ridge II from the origin, and is interpreted as being due to the cyclic structure (3.2) along the waves present in the data matrix.

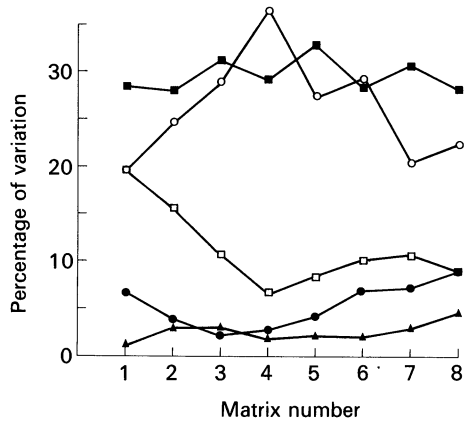

Fig. 5. Change in percentage contribution of the five principal features of the Thetford canopy height spectrum when calculated for successive 32 X 32 data matrices along the plot: I(a)–0; I(b)–●; II(a)–□; II(b)–■; III–▲.

Examination of the canopy height presence/absence data matrix shows blocks of zeros in rows forming a diagonal pattern at an angle of 163°. This corresponds to the direction along the waves; the wave direction is orthogonal, namely $\phi = 73°$. In comparison, the autocorrelation matrix contains two diagonal lines of elements with modulus near 0.1 from (5, 23) to (10, 6) and from (12, 7) to (16, −6), the corresponding ϕ values being $\tan^{-1}(17/5) = 73° 37'$ and $\tan^{-1}(13/4) = 72° 54'$. This common value of $\phi \sim 73°$ is very close to the ϕ value for the spectral ridges I and II, and the autocorrelation wave structure clearly reflects the same features in the data matrix as the spectral ridges.

3.5. *Stationarity*

We computed the censored-spectra of eight partially overlapping 32 x 32 sub-matrices of canopy heights $\{X_{st}^{(r)}\}$ ($r = 1, \ldots, 8$) with $c = 0.4$ per cent using rows 1–32, 12–43, . . ., 78–109. The percentage of variation explained was consistent throughout, and features present were similar to those described in Section 3.2. However, the percentage of variance attributable to the separate spectral entries varies with r. As the previously observed breaks in the ridge structures between low and high frequency components were found in all eight spectra, we consider the following component features: I(a)–low frequency, q positive ($0 \leqslant p \leqslant 9$); I(b)–high frequency, q positive ($10 \leqslant p \leqslant 16$); II(a)–low frequency, q negative ($0 \leqslant p \leqslant 11$); II(b)–high frequency, q negative ($12 \leqslant p \leqslant 16$); III– isolated entries.

As r is increased (Fig. 5), the most marked difference is a shift in the percentage of variation attributable to the low frequency components: I(a) reaches a maximum for $r = 4$, at which point II(a) reaches a minimum. The high frequency components are more stable, with II(b) showing slight oscillations and I(b) a shallow concave shape with a minimum at $r = 3$. The contribution of III remains low. As the data set is non-stationary then the overlapping sub-matrices are also non-stationary, and in this case our analysis is strictly invalid. However, as changes occur slowly and consistently across the site, for all practical purposes sub-matrix stationarity may be assumed.

These changes in the spectra reflect real changes in the structure of the forest. This site was being used for microclimatological measurements (Ford, 1976), and a large mast together with areas preserved for sensitive instruments was situated in rows 30–60. Two years previous to this canopy survey a light thinning was made, but there had been a tendency to remove fewer trees around the instrument mast and preserved areas and the changes in the spectrum across the plot can be interpreted in relation to this difference in thinning. Where there has been less thinning the

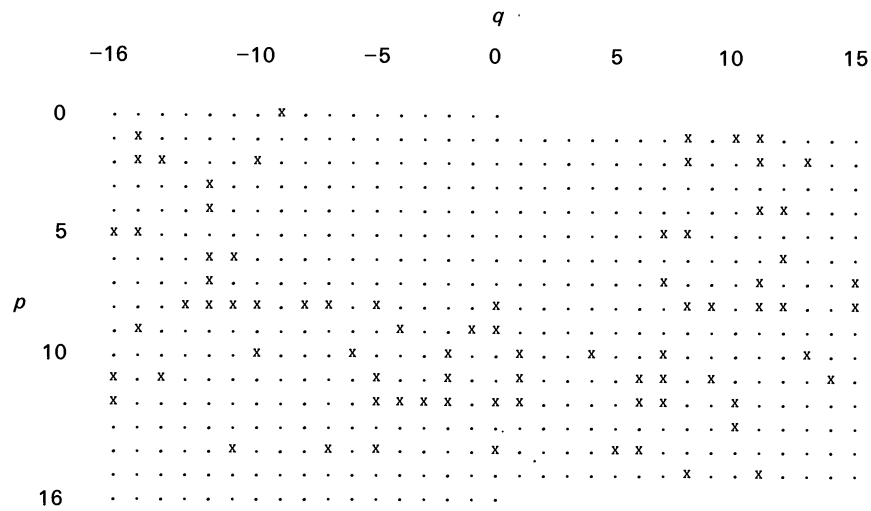

Fig. 6a. Point spectrum of Thetford tree positions in a 32 × 32 site away from the instrument mast, with X denoting elements contributing to at least 0.4 per cent of total variance. That of the approximating lattice spectrum is similar.

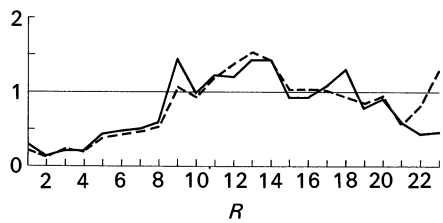

Fig. 6b. The scaled R spectrum of Thetford trunk positions from the same region as Fig. 5a: point spectrum, – – –; lattice spectrum, ——.

wave-like aggregation of tree crowns is strongest. The effect of planting in rows, feature II(b), remains virtually unaltered throughout.

3.6. *Analysis of Trunk Positions*

For tree-trunk positions both an exact analysis via the point spectrum (2.8) and analysis with (2.3) by approximating tree positions to the nearest points of a lattice are possible. In both cases the most notable feature of the spectrum (Fig. 6a) of a 32 × 32 site away from the instrument mast is a central region of approximate diameter 8 with low entries. To enable comparison the frequencies for the point spectrum were chosen to be the Fourier frequencies of the lattice spectrum. The scaled R spectra, for both point and lattice analyses, are given in Fig. 6b, and there is close agreement between them apart from two spurious peaks in the lattice spectrum at $R = 9$ and 18. This illustrates that considerable care is needed to ensure that the covering lattice structure is sufficiently fine.

As $\{2I_{pq}/\sigma^2\}$ are i.i.d. χ^2_2 random variables for independent $\{X_{st}\}$, any sum $\Sigma\,[2I_{pq}/\sigma^2]$ over m distinct values is distributed as χ^2_{2m} with expected value 2m. Thus if a scaled R band, the rth say, contains m values, then as the polar periodogram estimate R_r has expected value 1 it follows that R_r is distributed as (1/2m) χ^2_{2m}. Both R spectra have elements exceeding 1 for $11 \leqslant R \leqslant 14$;

and although the exact estimate R_{11} is not significant at the 10 per cent level, R_{12}, R_{13} and R_{14} are significant at the 2.5, 0.1, and 0.5 per cent levels, respectively. There is therefore strong evidence in support of spatial pattern over the frequencies $R = 12-14$ which correspond to wavelengths of 2.29–2.67 m. The presence of such pattern was anticipated as regularity of planting coupled with thinning policy suggested that nearest-neighbour distances generally lie in a fairly narrow band. Indeed these distances have lower, middle and upper quartiles of 2.51, 2.77 and 2.91 m, respectively, which are only slightly in excess of these values.

4. DISCUSSION

Evaluation of the Cartesian spectrum is the natural first attack on a data set, and we contend that it is the overall visual effect of spectra that is fundamentally important to interpretation and not the magnitude of individual entries, especially as the extent of spectral features must be subjective. From the analysis of forest structure it is apparent that the following processes are operating: (i) competition between trees; (ii) directional growth of tree crowns which has a major effect on the structure of the canopy not appreciated before the survey was made; and (iii) differences in management which, though small and not apparent during the survey, nevertheless influence structure. Quantifying the canopy structure with these techniques has proved of value in interpreting measurements of heat and water transfer made from this crop (Raupach, 1979). The three processes which interact and generate the pattern cannot be separated functionally from the analyses. For this a more comprehensive direct analysis of the processes of competition and crown growth would have to be made at a range of spacings and in particular over different ages of tree and forest.

Although the autocorrelation function and Cartesian spectrum are closely related (expression (2.2)), they transform the data in totally different ways. For example, Fig. 2 shows the canopy spectrum as two parallel ridges, whilst Fig. 4 shows the corresponding autocorrelations as a system of waves. As autocorrelations are themselves correlated, the autocorrelation function represents information in a more complex manner than the spectrum and hence is more difficult to interpret. However, when analysed in conjunction with the spectrum it may be of considerable use. For not only may it reinforce evidence of spatial structure suggested by the spectrum, but it may also indicate the presence of further structure not immediately apparent from the spectrum itself, the effect of canopy *absence* (Section 3.2) being a case in point.

Whilst the features contained in the forest canopy Cartesian spectrum are particularly striking, the same does not apply to other data sets we have examined. We have already seen that transformation to the polar R spectrum concentrates the information content into concentric annuli around the origin, and the smoothing of the resultant scaling operation enables the detection of quite small effects which may not be immediately apparent from the Cartesian spectrum. In a subsequent paper we shall present various spectral analyses of these other data sets and show in particular that the polar θ spectrum is powerful in the detection of anisotropy, a most useful feature for the potential model-builder. For most growth processes in the natural environment are subject to some degree of directional influence, and it is of considerable importance that the presence of any resulting anisotropy within a sample data set is detected in the initial interrogation.

REFERENCES

Bartlett, M. S. (1964) The spectral analysis of two-dimensional point processes. *Biometrika*, **51**, 299–311.

——— (1975) *The Statistical Analysis of Spatial Pattern*. London: Chapman and Hall.

——— (1978) *An Introduction to Stochastic Processes*, 3rd ed. London: CUP.

Branch, J. L. (1973) Two-dimensional forward Chirp discrete Fourier transform. Imperial College, London.

Cliff, A. D. and Ord, J. K. (1981) *Spatial Autocorrelation*. London: Pion.

Cochrane, L. A. and Ford, E. D. (1978) Growth of a sitka spruce plantation: analysis and stochastic description of the development of the branching structure. *J. Appl. Ecol.*, **15**, 227–244.

Ford, E. D. (1976) The canopy of a Scots pine forest: description of a surface of complex roughness. *Agric. Met.*, **17**, 9–32.

Ford, E. D. and Deans, J. D. (1978) The effects of canopy structure on stem flow, throughfall and interception loss in a young Sitka spruce plantation. *J. Appl. Ecol.*, **15**, 905–917.

Huang, T. S. (1972) Some two-dimensional windows. *IEEE Trans. on A and E*, **AU-20**, No. 1, 88–89.

Jenkins, G. M. and Watts, D. G. (1968) *Spectral Analysis and its Applications*. San Francisco: Holden-Day.

Lugt, A. V. (1974) Coherent optical processing. *Proc. of the IEEE*, **62**, 1300–1319.

McBratney, A. B. and Webster, R. (1981) Detection of ridge and furrow pattern by spectral analysis of crop yield. *Int. Stat. Rev.*, **49**, 45–52.

Mercer, W. B. and Hall, A. D. (1911) The experimental error of field trials. *J. Agric. Sci.*, **4**, 107–132.

Monro, D. M. (1971) Complex discrete fast Fourier transform in two dimensions. Imperial College, London.

——— (1975) Algorithm AS 83. Complex discrete fast Fourier transform. *Appl. Statist.*, **24**, 153–160.

Monro, D. M. and Branch, J. L. (1977) Algorithm AS 117. The Chirp discrete Fourier transform of general length. *Appl. Statist.*, **26**, 351–361.

Priestley, M. B. (1964) The analysis of two-dimensional stationary processes with discontinuous spectra. *Biometrika*, **51**, 195–217.

Rabiner, L. R. and Gold, B. (1975) *Theory and Application of Digital Signal Processing*. New Jersey: Prentice-Hall.

Raupach, M. R. (1979) Anomalies in flux-gradient relationships over forest. *Boundary-Layer Meteorol.*, **16**, 467–486.

Ripley, B. D. (1981) *Spatial Statistics*. New York: Wiley.